Article

The Impact of Quality Control Methods on Vegetation Monitoring Using MODIS FPAR Time Series

Kai Yan [1], Xingjian Zhang [2], Rui Peng [3], Si Gao [1,3] and Jinxiu Liu [2,*]

1 Innovation Research Center of Satellite Application (IRCSA), State Key Laboratory of Remote Sensing Science, Faculty of Geographical Science, Beijing Normal University, Beijing 100875, China; kaiyan@bnu.edu.cn (K.Y.); gaosi_gs@163.com (S.G.)
2 School of Information Engineering, China University of Geosciences, Beijing 100083, China; xingjianzhang@email.cugb.edu.cn
3 School of Land Science and Techniques, China University of Geosciences, Beijing 100083, China; ruipeng213@gmail.com
* Correspondence: jinxiuliu@cugb.edu.cn

Abstract: Monitoring vegetation dynamics (VD) is crucial for environmental protection, climate change research, and understanding carbon and water cycles. Remote sensing is an effective method for large-scale and long-term VD monitoring, but it faces challenges due to changing data uncertainties caused by various factors, including observational conditions. Previous studies have demonstrated the significance of implementing proper quality control (QC) of remote sensing data for accurate vegetation monitoring. However, the impact of different QC methods on VD results (magnitude and trend) has not been thoroughly studied. The fraction of absorbed photosynthetically active radiation (FPAR) characterizes the energy absorption capacity of the vegetation canopy and is widely used in VD monitoring. In this study, we investigated the effect of QC methods on vegetation monitoring using a 20-year MODIS FPAR time series. The results showed several important findings. Firstly, we observed that the Mixed-QC (no QC on the algorithm path) generally produced a lower average FPAR during the growing season compared to Main-QC (only using the main algorithm). Additionally, the Mixed-QC FPAR showed a very consistent interannual trend with the Main-QC FPAR over the period 2002–2021 ($p < 0.05$). Finally, we found that using only the main algorithm for QC generally reduced the trend magnitude ($p < 0.1$), particularly in forests. These results reveal differences in FPAR values between the two QC methods. However, the interannual FPAR trends demonstrate greater consistency. In conclusion, this study offers a case study on evaluating the influence of different QC methods on VD monitoring. It suggests that while different QC methods may result in different magnitudes of vegetation dynamics, their impact on the time series trends is limited.

Keywords: vegetation dynamic (VD); fraction of absorbed photosynthetically active radiation (FPAR); trend analysis; MODIS; quality control (QC)

1. Introduction

As a crucial part of the carbon cycle and energy balance in terrestrial ecosystems, vegetation serves as an indicator of how ecosystems respond to climate change and human activities [1–4]. Vegetation not only plays an important role in climate regulation, carbon cycling, and hydrological processes but also contributes to soil conservation and reduces greenhouse gas emissions [5–7]. However, in the face of global warming, increasing human activities have had a significant impact on global vegetation, making it an urgent issue in discussions about global change [8–12]. Accurately monitoring and assessing vegetation dynamics (VD) over extended periods, as well as identifying the driving mechanisms, is crucial for gaining a comprehensive understanding of human activities, climate change, and the interactions between vegetation and ecosystems [13–16]. This understanding has

important implications for our ability to predict, mitigate, and adapt to future global climate change and its impacts [17,18].

The Northern Hemisphere is characterized by a wide and diverse range of ecosystems and vegetation types that play an important role in the global carbon cycle, climate change, and the water cycle [19–21]. Studying the VD in the Northern Hemisphere is crucial for understanding how global vegetation responds and adapts to climate change. This understanding has led to a large number of studies on the VD in the Northern Hemisphere [22–25]. Satellite remote sensing has greatly improved our ability to monitor global VD due to its long-term series, short observation intervals, and wide coverage [18,26]. There are remote sensing products available with different spatial and temporal resolutions, as well as various application scenarios, which provide a wealth of valuable information for monitoring VD and analyzing its driving factors at multiple scales and over long periods [27–29]. These products include vegetation indices, vegetation parameters, vegetation productivity, climate variables, and land cover products. They offer valuable insights into vegetation structure, health status, change trends, and climate response and regulation, enabling us to gain a comprehensive and quantitative understanding of global VD in space and time [15,18,30–32].

The fraction of absorbed photosynthetically active radiation (FPAR) is defined as the ratio of vegetation's absorption of solar radiation energy at wavelengths between 400 nm and 700 nm. This ratio characterizes the strength of vegetation's photosynthetic capacity [33–35]. The FPAR is an essential climate variable (ECV) recognized by the United Nations Global Climate Observing System (GCOS) [36] and is an important biophysical variable that characterizes the exchange of energy, mass, and momentum between vegetation and the atmosphere [37]. The FPAR is closely linked to various factors, such as vegetation species, leaf chlorophyll content, leaf area index (LAI), leaf inclination distribution, solar altitude angle, and skylight conditions [38–40]. Therefore, the FPAR provides crucial information about the rate of vegetation photosynthesis, which affects the exchange of energy and carbon between the biosphere and the atmosphere [41]. Monitoring and evaluating FPAR dynamics are crucial for understanding changes in vegetation productivity, climate change impacts, and overall vegetation health [29,42,43].

However, input reflectance data for FPAR retrieval sometimes have high uncertainties due to poor observational conditions, such as cloud/aerosol contamination, large-angle observations, snow and ice cover, and sub-optimal atmospheric corrections [44–47]. As a result, the "best" retrieval algorithms for many FPAR products are often not realized. Instead, only "backup" algorithms with less precision, accuracy, and stability are used and flagged in the quality layer [47–50]. Due to their advantages, such as a clear theoretical basis, relatively high spatial and temporal resolution, and free access, MODIS FPAR products have been widely used in various fields since they were first released in 2000 [29]. In the MODIS FPAR product, the operational algorithms include a main algorithm based on the radiative transfer (RT) model and a backup empirical method based on relations between the normalized difference vegetation index (NDVI) and the FPAR [48]. However, if the solar observation zenith angle is too large, the atmospheric correction is not ideal, or the surface is covered by snow and ice, the bidirectional reflectance factor (BRF) may have large uncertainty, and the accuracy of the radiative transfer model will be reduced. This leads to the failure of the main algorithm and the execution of the backup algorithm [44,48,51,52]. Additionally, an inaccurate input biome classification map can also cause the main algorithm to fail [44]. Therefore, the MODIS FPAR product includes retrieval results for two different algorithm paths and provides the algorithm paths as critical quality control (QC) information to the user [44,53–55].

The QC information provides information about the relative reliability and accuracy of the remote sensing products. Researchers can use this information to filter the inversion results with higher quality, thereby improving the reliability of the research results or developing improved re-analysis datasets based on QC [49,56–61]. However, as an important source of uncertainty in remote sensing products, differences in QC may lead

to less reliable vegetation monitoring results or even contradictory conclusions [18,62–65]. Although research has been conducted on the impact of MODIS products' QC on specific applications [66,67], there is still a lack of research on the impact of QC on long-term vegetation change. Therefore, there is an urgent need to understand how remote sensing products under different QC methods affect vegetation monitoring over long time series to ensure the reliability of related studies such as "Greening the Earth". This study aims to address the following three issues using the example of the MODIS C6.1 FPAR time series from 2002–2021. First, whether there is a systematic overestimation or underestimation of FPAR values with QC versus without QC. Second, while the QC information clearly indicates the presence of a low-quality FPAR, does this lead to a fundamental change in the trend direction of the time series data? Finally, whether there is a difference in trend magnitude between the FPAR with QC and without QC. To address these issues, we compared the magnitude of the different QC FPARs and used the Mann–Kendall (MK) test, Sen's slope method, and linear trend analysis to statistically analyze the long-term trends of the FPAR in the Northern Hemisphere growing season under different QC methods. This study can reveal the long time series trend of the vegetation FPAR in the Northern Hemisphere and guide the use of global vegetation products.

2. Materials and Methods

2.1. Study Area

The study area includes the entire Northern Hemisphere north of the equator. This includes North America, Europe, most of Asia, the northern half of Africa, and northern South America. The region's diverse climatic types, topographic distribution, precipitation, and temperature have given rise to various vegetation types. These include eight biome types: grasses/cereal crops, shrubs, broadleaf crops, savannas, evergreen broadleaf forests (EBF), deciduous broadleaf forests (DBF), evergreen needleleaf forests (ENF), and deciduous needleleaf forests (DNF) [68]. The distribution and percentage of each biome type can be seen in Figure 1. In this study, we used the growing season averaged FPAR (GSA FPAR) for our analysis. Referring to previous studies [69,70], we defined the vegetation growing season in the Northern Hemisphere as May through September each year. This period is the peak of vegetation growth and selecting it as the study time frame allowed us to concentrate on the critical period of vegetation growth.
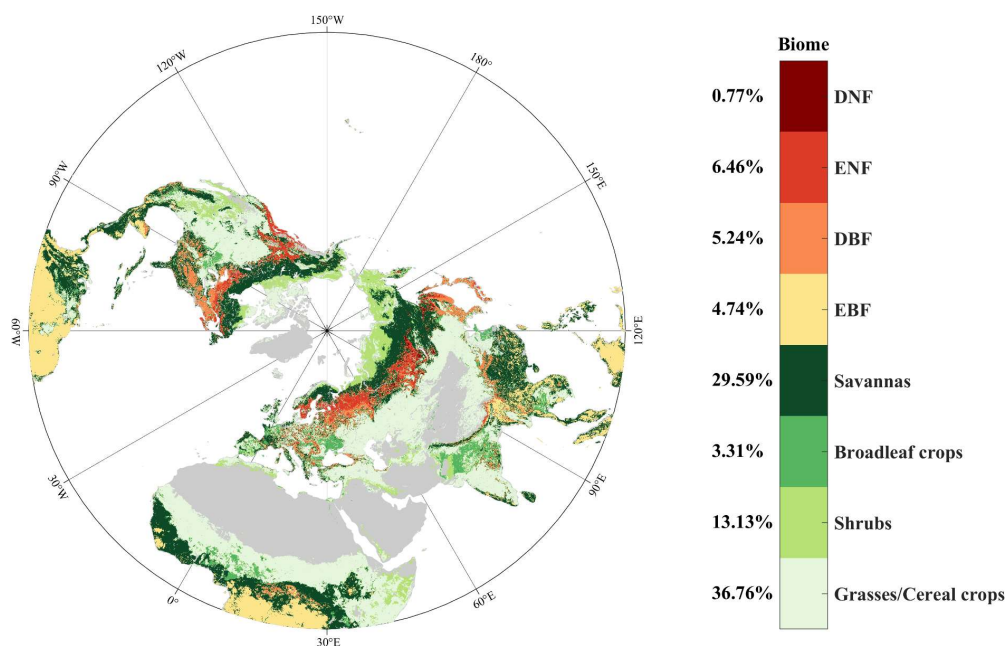

Figure 1. Biome coverage map of the study area in 2021.

2.2. Datasets

2.2.1. MODIS FPAR Product

The FPAR data used in this study are the MODIS C6.1 FPAR product (MOD15A2H) with a time interval of 8 days and a raw spatial resolution of 500 m [71]. In the QC layer of this product, the algorithm path of this FPAR product is divided into a main algorithm based on the RT model and a backup algorithm based on the empirical relationship between the FPAR-NDVI [48]. The operational retrieval algorithm first executes the main algorithm, which is flagged as saturated (Main-S) if the input reflectance is oversaturated in the case of a high-density canopy. If the uncertainty of input reflectance is greater than a threshold or the sun–sensor geometry is bad, the main algorithm may not find a solution. In this case, the backup algorithm with lower accuracy is executed [44]. Based on this algorithm information, we categorize the MODIS FPAR QC methods into two types: only using the main algorithm retrievals (Main-QC) and using both main and backup algorithm retrievals (Mixed-QC). All MODIS FPAR products are available via LP DAAC (https://lpdaac.usgs.gov/products/mod15a2hv061/, accessed on 20 December 2023).

2.2.2. MODIS Land Cover Product

The MCD12Q1 C6.1 product is the latest MODIS land cover product obtained from a supervised classification using MODIS Terra and Aqua observations. The map projection for this product is the same as the FPAR product. For the purpose of this study, we utilized LC_Type3 (Land Cover Type 3: Annual LAI Classification) for vegetation type classification [68]. The MCD12Q1 C6.1 product is available via LP DAAC (https://lpdaac.usgs.gov/products/mcd12q1v061/, accessed on 21 December 2023).

2.3. Methods

This study is based on MODIS C6.1 FPAR products and MODIS C6.1 land cover products for the Northern Hemisphere. The main steps include (1) data pre-processing and (2) trend analysis. The specific technical route is shown in Figure 2.
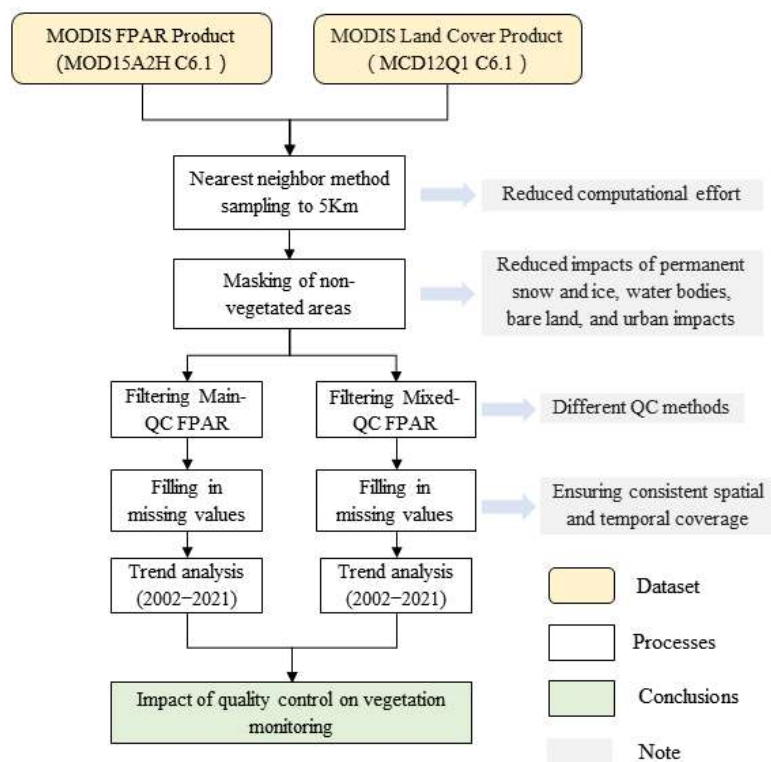

Figure 2. Flowchart of QC analysis of the MODIS FPAR time series for vegetation monitoring in the Northern Hemisphere.

2.3.1. Data Pre-Processing

In this study, we first reduced the amount of data by decreasing the spatial resolution to 5 km $\times$ 5 km using the nearest-neighbor sampling method for computational efficiency. Second, we masked the non-vegetated areas of each dataset (water bodies, bare land, and cities) using MCD12Q1 for each year to minimize the effects of permanent snow and ice. Then, we separately screened the Main-QC FPAR and the Mixed-QC FPAR to obtain the MODIS FPAR time series under the two QC methods. In addition, to ensure more consistent spatial and temporal continuity between the two sets of time series data, we filled in missing data using simple arithmetic averaging in climatology. This method calculates the multiyear mean for the same period to fill in the gaps for each period of each time series [72]. In this study, the data used for filling were the 20-year mean from 2002 to 2021.

Finally, we extracted the GSA FPAR for each year from the pre-processed MODIS FPAR data as the analyzed data, which can be calculated using the following formula:

$$\text{GSA FPAR} = \frac{\sum_{i=n}^{n+16} \text{FPAR}_i}{16}, \tag{1}$$

$$\text{GSA}_\text{B} \text{ FPAR} = \frac{\sum_{j=1}^{k} (\text{GSA FPAR})_j}{k}, \tag{2}$$

where GSA FPAR represents the average FPAR of 16 composites for a given pixel over the growing season, GSA_B FPAR represents the average FPAR for the entire Northern Hemisphere for a given vegetation type, i represents the i-th composite of the FPARs for the growing season, and k represents the number of pixels for that vegetation type B.

2.3.2. Trend Analysis Methods

In this study, we conducted a linear trend analysis to examine the long-term trends in the GSA_B FPAR for eight vegetation types in the Northern Hemisphere vegetation zone from 2002 to 2021. The slope of the linear regression equation was used to represent the interannual trend of the FPAR. Significance was evaluated using a t-test and classified ($p < 0.001$), significant ($p < 0.05$), and weakly significant ($p < 0.1$). The MK test is a trend analysis tool recommended by the World Meteorological Organization (WMO) [73]. It was first proposed by Mann and reformulated by Kendall in a way that does not require assuming a particular form of the data distribution function [74,75]. In the MK test, a positive value of the MK statistical indicator (Z) indicates an upward trend, and a negative value indicates a downward trend. The trend in the time series data was tested at a significance level α. When $|Z|$ is greater than or equal to 1.64 ($\alpha = 0.1$), 1.96 ($\alpha = 0.05$), and 2.58 ($\alpha = 0.01$) in the MK test, this means that the time series passes the significance test at the confidence level of 90%, 95%, and 99%, respectively. In this paper, we selected $\alpha = 0.1$ in order to obtain as much comparison data as possible.

In this study, the magnitude of the trend is assessed using Sen's estimator of the slope [76] and calculated using the following formula:

$$S_i = \frac{x_b - x_a}{b - a} i = 1, \dots, N, \tag{3}$$

where x_a and x_b represent the time series values at time points a and b, respectively (where $b > a$). The median of the N values for S_i was taken to obtain the Sen's slope estimator. A positive value for the Sen's slope estimator indicates an upward trend in the time series, while a negative value indicates a downward trend.

3. Results

3.1. Comparison of FPAR Spatial Distributions

The multiyear mean GSA FPAR from 2002 to 2021 showed that the Mixed-QC FPAR was lower than or equal to the Main-QC FPAR for 99.23% of Northern Hemisphere vegetation (Figure 3a). Among these, approximately 50.67% of the Mixed-QC FPAR had

smaller values compared to the Main-QC algorithm, while around 48.56% were nearly equal. The Mixed-QC algorithm primarily underestimated the FPAR compared to the Main-QC algorithm in high-latitude areas and tropical rainforests. However, there were a few areas at the southern edge of the Sahara Desert where the Mixed-QC FPAR exhibited higher values than the Main-QC. The smallest average difference in the FPAR was observed between 30° N and 50° N, while the largest differences were found between 18° N and 30° N and between 0° and 10° N (Figure 4a). Therefore, without controlling for the algorithm path, regions such as high latitudes and tropical rainforests had slightly lower mean FPAR values compared to the Main-QC. This difference can be attributed to the incorporation of more FPAR data from the backup algorithm, which has been shown in previous studies to underestimate the main algorithm [77].
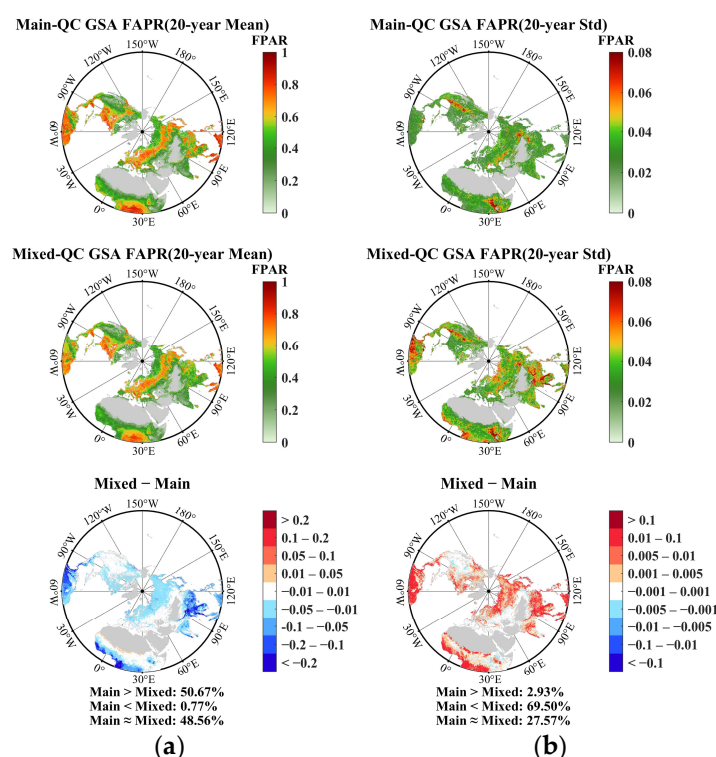

Figure 3. Spatial distribution of the GSA FPAR in the Northern Hemisphere under different QC methods: (**a**) multiyear mean of the GSA FPAR for 2002–2021 and (**b**) standard deviation of the multiyear GSA FPAR for 2002–2021. The first row represents the result of the Main-QC, the second row represents the result of the Mixed-QC, and the third row represents the result of the Mixed-QC minus Main-QC. The white areas on the land surface indicate that the differences between the two QC methods are small and negligible.

Furthermore, we computed the standard deviation of the multiyear GSA FPAR over 20 years (Figure 3b). The analysis revealed that the overall standard deviation of the Mixed-QC FPAR was equal to or greater than that of the Main-QC, representing 97.07% of the total vegetated pixels. Among them, approximately 69.5% of the Mixed-QC FPAR had higher values than the Main-QC, while around 27.57% were approximately equal. Spatially, the regions with higher mixed FPARs compared to the Main-QC were primarily located in high-latitude and tropical areas. When examining the average differences in standard deviation based on latitude, the smallest discrepancy was observed between 30° N and 50° N, while the largest discrepancies were found between 18° N and 30° N and between 0° and 10° N (Figure 4b). This may be due to the presence of a higher frequency of cloudy and rainy weather in the tropical region during the growing season period, which leads to a decrease in the quality of the observations in this region and brings more low-quality backup algorithm FPAR data. These results suggest that backup algorithm FPAR data

without controlling the algorithm path increases the variability and decreases the stability of the time series data.
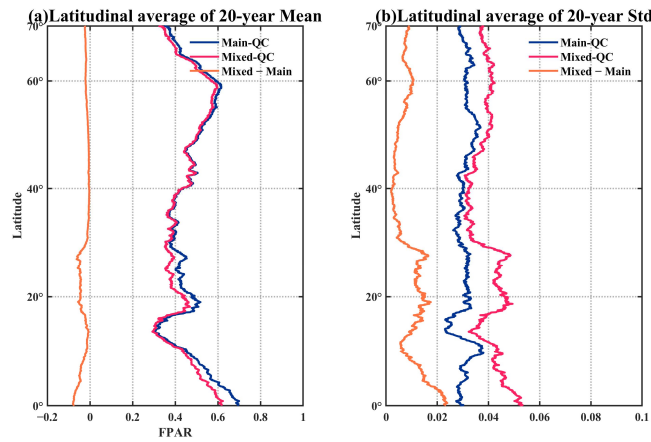

Figure 4. Latitudinal differences under different QC methods in: (**a**) the multiyear mean GSA FPAR and (**b**) the multiyear GSA FPAR standard deviation.

3.2. Comparison of FPAR Histograms

The Mixed-QC exhibits a lower multiyear mean GSA FPAR and higher standard deviations compared to the Main-QC (Figure 5). For non-forest vegetation, the frequency histogram curves of the FPAR for both methods exhibit similar distribution patterns. Specifically, within the grasses/cereal crops category, the frequency histogram curves of the two methods almost overlap, with nearly equal standard deviations. However, the Mixed-QC FPAR is slightly lower (0.315 vs. 0.32). The largest differences are observed for the shrub vegetation type, where the curve of the Main-QC peaks slightly to the right, and the average FPAR is higher than that of the Mixed-QC (0.382 vs. 0.408).
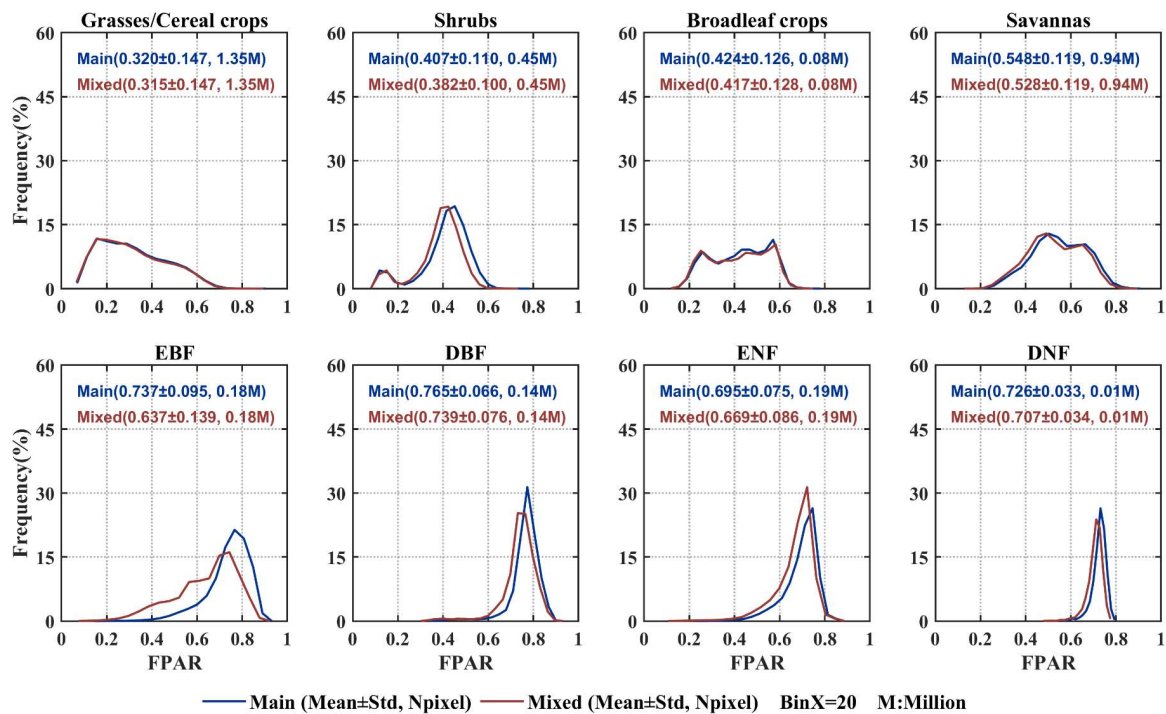

Figure 5. The histogram curves demonstrate the frequency distribution of the multiyear mean GSA FPAR under different QC methods. Pixels were masked from 2002 to 2021 when vegetation types transitioned to other types. In addition, pixels with valid values under both QC methods were selected for statistical analysis.

In forests, the Mixed-QC still exhibits lower a multiyear mean GSA FPAR and higher standard deviations. However, the differences were significantly greater in forests compared to non-forest types. Specifically, in the frequency distribution histogram curves of the EBF, DBF, and DNF types, the Mixed-QC shows a leftward shift and lower peak positions compared to the Main-QC. The largest difference is observed in the EBF vegetation type, where the Mixed-QC has a lower FPAR than the Main-QC (0.637 vs. 0.737), and a larger standard deviation (0.139 vs. 0.095). The smallest difference is observed in the DNF type, where the Mixed-QC FPAR is only slightly lower by 0.019 (0.707 vs. 0.726), and the standard deviation is only slightly higher by 0.001 (0.034 vs. 0.033).

3.3. Comparison of 20-Year FPAR Trends

The annual GSA_B FPAR for the Northern Hemisphere followed a similar trend for both QC methods from 2002 to 2021 (Figure 6). However, the Mixed-QC consistently had smaller annual GSA_B FPAR compared to the Main-QC for each corresponding year. Notably, grasses/cereal crops, broadleaf crops, and savannas showed a highly significant increase in annual GSA_B FPAR for all three non-forest vegetation types ($p < 0.001$). In the shrubs type, the Main-QC exhibited a highly significant increase ($p < 0.001$), while the Mixed-QC showed a significant increase ($p < 0.05$). The annual growth rate of the Mixed-QC FPAR was slightly higher than that of the Main-QC for all four vegetation types. In forest vegetation, the Mixed-QC still had a smaller annual GSA_B FPAR than the Main-QC, with the largest difference observed in the EBF type. In terms of trend, both QC methods showed significant increases ($p < 0.05$) for all three vegetation types, except for EBF, where the Main-QC had a slightly larger slope than the Mixed-QC for DBF vegetation and the Main-QC had a slightly smaller slope than the Mixed-QC for ENF and DNF vegetation.
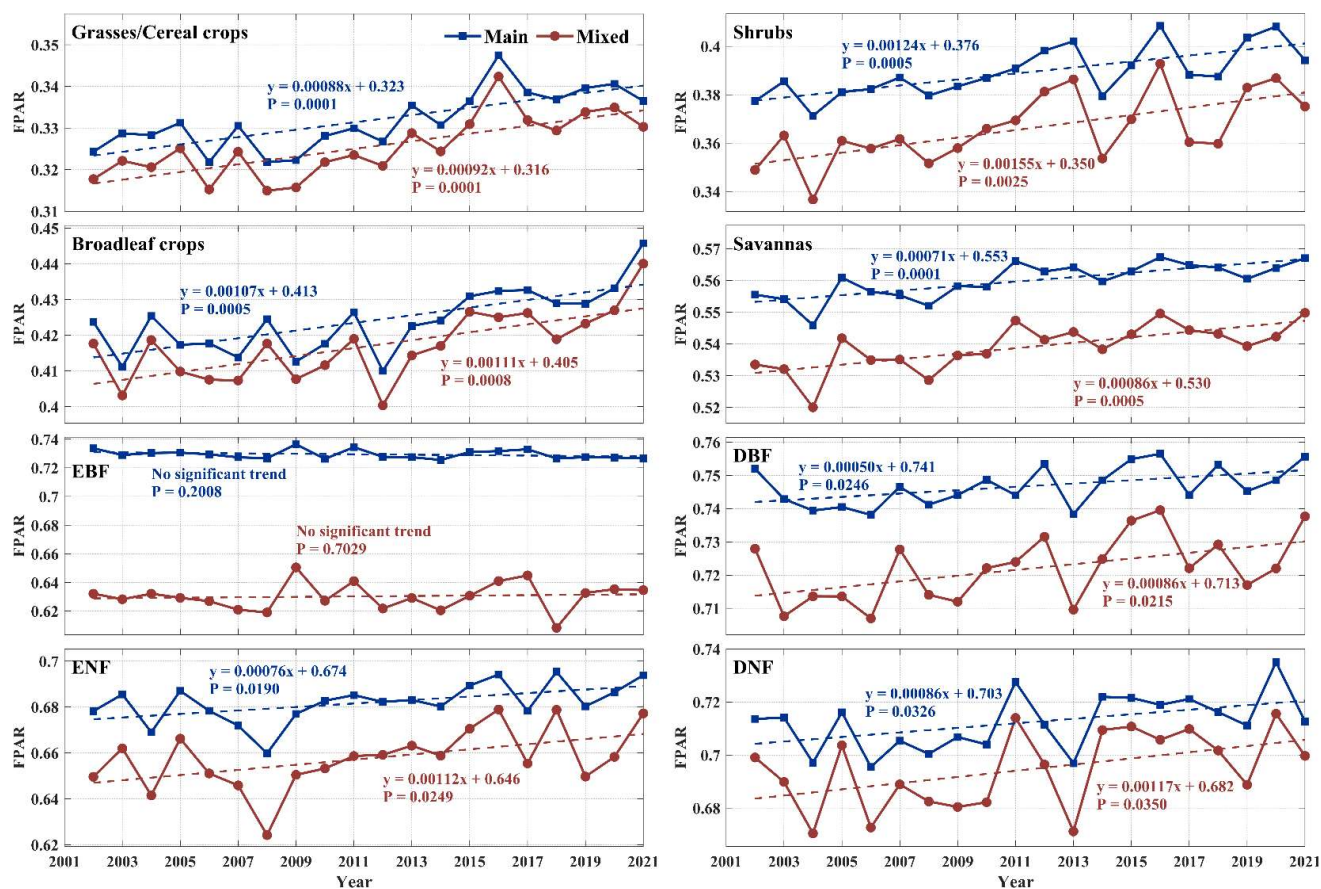

Figure 6. The interannual trends of the Main-QC GSA_B FPAR and the Mixed-QC GSA_B FPAR in the Northern Hemisphere from 2002 to 2021.

The GSA FPAR values between the Main-QC and Mixed-QC were generally consistent across most regions from 2002 to 2021 (Figure 7). Without the MK test, approximately 59.35% of the vegetated area showed almost equal annual changes between the Main-QC and Mixed-QC, with noticeable differences concentrated in tropical and high latitude regions (Figure 7a). After conducting the MK trend test, the areas that passed the trend test were similar for both QC methods (32.5% vs. 29.72%, $p < 0.1$), and the areas with significant changes were highly consistent (Figure 7b). Among these areas, approximately 27.79% and 25.42% of the pixels showed a significant increase for the Main-QC and Mixed-QC, respectively, primarily in Asian regions such as China and India, consistent with existing research [78]. The proportion of pixels with a significant decrease was 4.7% and 4.3% for the Main-QC and Mixed-QC, respectively, mainly located in regions on the edge of the Sahara Desert. In terms of trend magnitude, approximately 63.43% of the regions showed similar trends between the Main-QC and Mixed-QC, while the Main-QC had a greater trend magnitude in 29.18% of the regions, and a smaller trend magnitude in 7.39% of the regions.
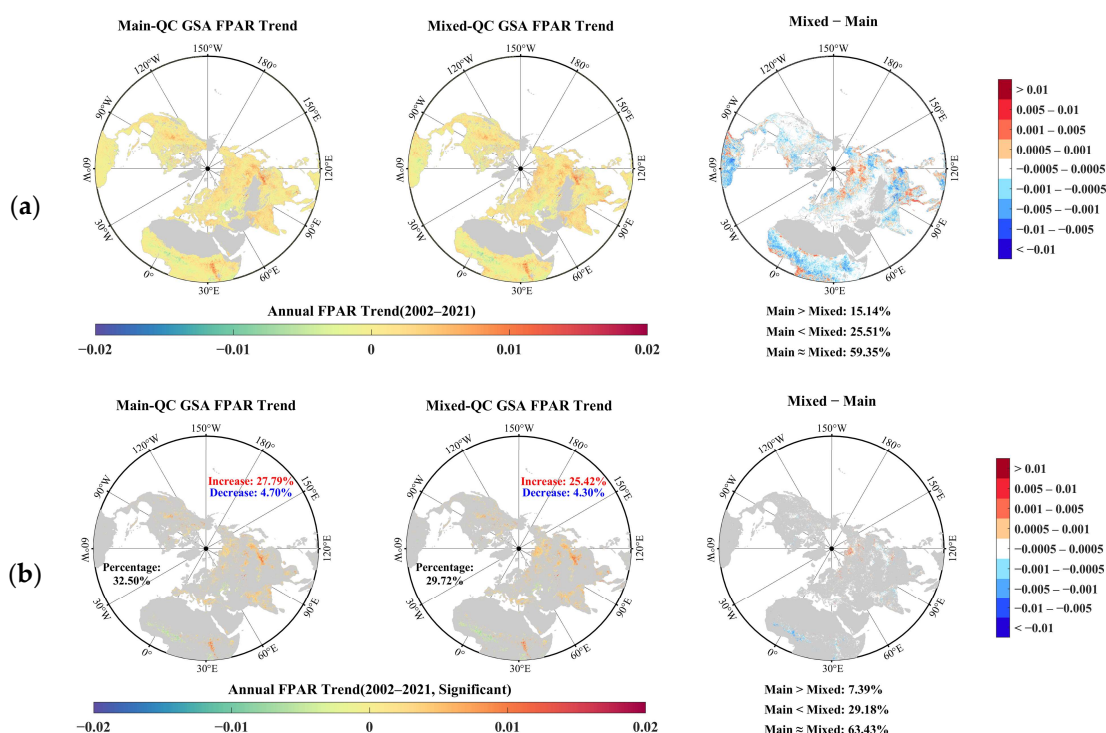

Figure 7. Spatial distribution of Northern Hemisphere GSA FPAR trends and their differences for different QC methods. (**a**) The trend estimates were based on Sen's slopes. (**b**) The trend estimates that passes the MK significance test. Only pixels with a statistical test (Z) greater than or equal to 1.64 and a significance level greater than 90% are retained here. The white areas on the land surface vary less and can be considered roughly equal.

The frequency distribution of the trend magnitude shows a significant difference between the Main-QC and Mixed-QC under EBF vegetation, while the remaining seven vegetation types are more consistent (Figure 8). Overall, the mean trend magnitude and standard deviation were slightly higher for the Mixed-QC compared to the Main-QC, but the number of pixels passing the MK test was lower for the Mixed-QC. In non-forested vegetation, the histogram curves for grasses/cereal crops and broadleaf crops almost overlapped, with similar mean trend magnitudes and standard deviations under both QC methods. However, the shrubs type showed significant variation, with the Mixed-QC having a slightly rightward and smaller peak in the curve, as well as a higher mean trend magnitude and standard deviation compared to the Main-QC (0.0036 ± 0.0016 vs. 0.0028 ± 0.0013). In forests, the differences in the frequency distribution of trend magnitude

were more pronounced. EBF exhibited the largest difference, with the Mixed-QC showing a wider bandwidth, lower peaks, peaks shifted away from 0, and a larger mean and standard deviation compared to the Main-QC (0.0012 ± 0.0047 vs. 0.0004 ± 0.0022). Additionally, we plotted the percentage of trends for different vegetation types under the two QC methods over 20 years from 2002 to 2021 (Figure 9). The results showed that the percentage of significant increase in the FPAR was higher for the Main-QC, except for B8 (DNF). The percentage of a significant decreasing trend was similar between the Main-QC and Mixed-QC, except for B6 (DBF), B7 (ENF), and B8 (DNF).
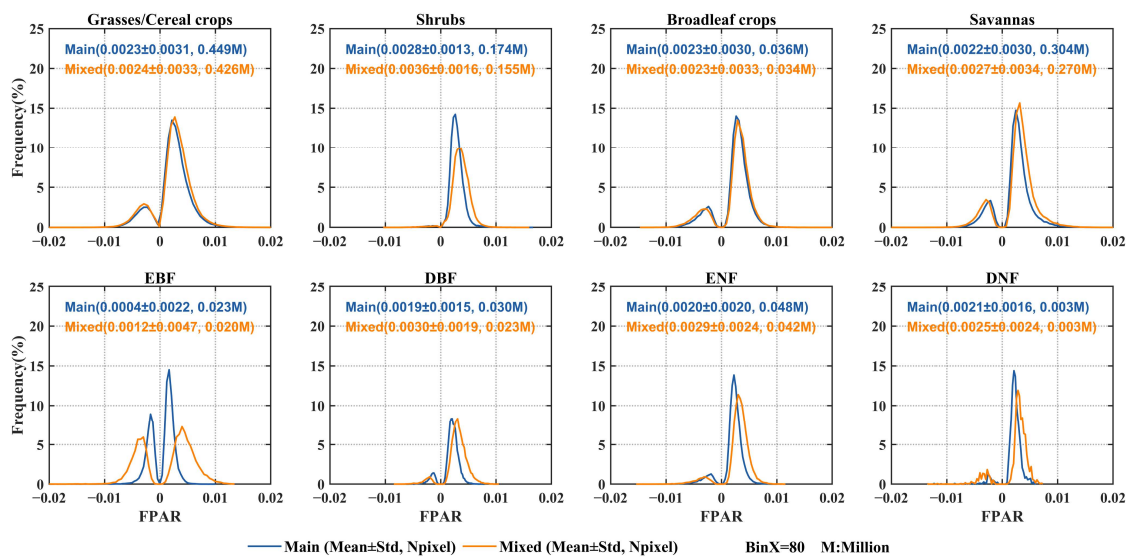

Figure 8. The frequency distribution of GSA FPAR trends in the Northern Hemisphere under different QC methods. Only pixels that showed no change in vegetation type between 2002 and 2021 and passed the MK significance test were selected for statistical analysis.
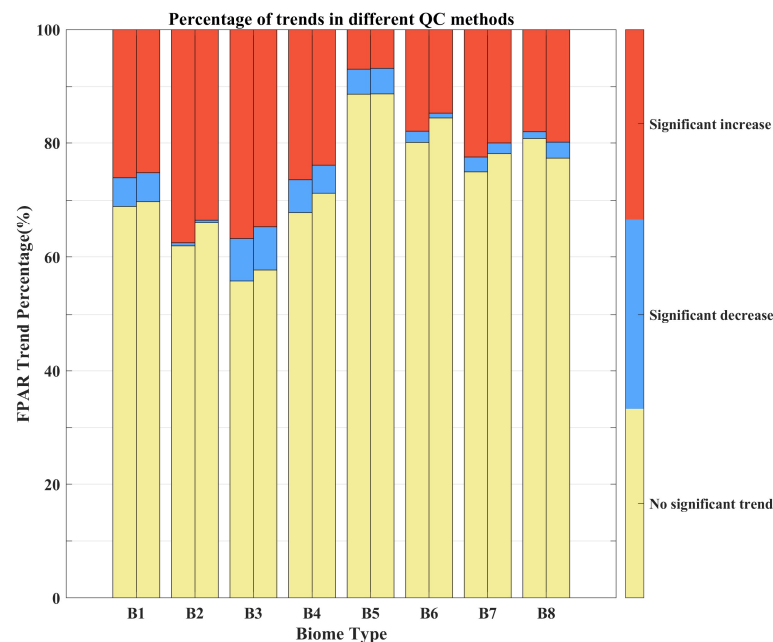

Figure 9. Percentage of four trends (no significant trend, significant decrease, and significant increase) in the GSA FPAR under different QC methods between 2002 and 2021. The trend was categorized as no significant trend if it did not pass the significance test or passed the significance test but the absolute value of the change was less than 0.001 and as a significant increase (decrease) if it passed the significance test and the absolute value of the change was greater than 0.001.

4. Discussion

4.1. Understanding the Inconsistency in Different Quality Control Methods

From the comprehensive evaluation of the above sections, we can conclude that in the trend test for long time series, the Main-QC FPAR and Mixed-QC FPAR have the same trend direction, but there are differences in the values and trend magnitude. For the MODIS FPAR product, due to the lack of quality control, the Mixed-QC FPAR includes a backup algorithm FAPR in addition to the main algorithm FPAR [71]. The backup algorithm is derived by establishing an empirical relationship between the main algorithm FAPR and the corresponding NDVI [79]. Empirical methods have few parameters, are simple and efficient to compute, but the vegetation index itself is affected by factors such as soil background, observation angle, atmospheric conditions, and saturation effects, resulting in the high uncertainty of the algorithm [80–83]. As a result, the backup algorithm has lower inversion accuracy and reliability than the main algorithm, which will lead to greater volatility (higher Std) in the Mixed-QC FPAR time series as well as differences in both FPAR values and trend magnitude between the two QC methods. Previous studies have shown that the backup algorithm underestimates the FAPR with respect to the FPAR of the main algorithm [77]. However, this underestimation appears to be systematic, in that the direction of the trend in the time-series data is very consistent despite the differences in values and trend magnitudes.

4.2. Impact of Quality Control on Vegetation Monitoring

The results of this study provide valuable insights into the effects of different QC methods on VD in the Northern Hemisphere from 2002 to 2021. We observed a consistent and significant trend in the FPAR across different QC methods. However, we found some notable differences in the GSA FPAR, areas of significant change, and trend magnitude across the QC methods. One important finding is that the Mixed-QC FPAR consistently showed smaller values compared to the corresponding Main-QC. This discrepancy is attributed to the backup algorithm underestimating the FPAR when compared to the main algorithm [77]. This underestimation is detrimental to assessing the impact of factors such as land use management, short-term climate change, etc., on the FPAR, as a lower or higher FPAR may be due to QC. This may interfere with the designation of land use management policies. The lower precision of the backup algorithm also contributes to a larger standard deviation in the multiyear Mixed-QC GSA FPAR, exacerbating the variability in the MODIS FPAR time series.

Furthermore, we examined the area of significant change and trend magnitude for both Main-QC and Mixed-QC methods. The Main-QC exhibited a larger area (32.50%) of significant change compared to the Mixed-QC (29.72%). Regarding the trend magnitude, the Mixed-QC generally showed slightly larger trends in the FPAR compared to the Main-QC, both in the interannual FPAR time series analysis and pixel-by-pixel trend analysis. For instance, in the interannual FPAR time series of Shrubs, the Mixed-QC exhibited an annual growth magnitude 25% higher than the Main-QC (Figure 6). Similarly, in the pixel-by-pixel trend analysis of the ENF trend, the Mixed-QC displayed an average annual growth magnitude 45% higher than the Main-QC (Figure 8).

In existing long-term vegetation monitoring studies, researchers tend to place more emphasis on the overall trend of vegetation (whether it is turning green or brown), the drivers of change, and the response and regulation of vegetation to climate [30,32,84–88]. The determination of the change area is often given as an approximate range. This is because it is very difficult to accurately and unambiguously determine vegetation change through remote sensing. In addition, it is more important to know the direction of vegetation trends and the driving factors behind them than to accurately determine the area or trend magnitude in order for humans to understand and respond to global climate change, formulate appropriate policies for sustainable development, and improve and refine land-use management [78,89–92]. However, despite the limited influence of different QC methods on the monitoring of long time series vegetation trends, we still recommend

referring to the QC documents of remote sensing products and selecting high-quality inversion results for the study, which can enhance the reliability and accuracy of the study to a limited extent. In addition, studies can be carried out using reanalyzed datasets with higher product quality, better spatial and temporal continuity, and more internal consistency compared to the original ones [60,61,93].

4.3. Limitations and Future Works

When performing QC on the product, it inevitably disrupts the data both in terms of time and space. Therefore, to ensure that the two QC methods have relatively consistent continuity in both time and space, we filled in the missing data in the time series of the two QC methods during the preprocessing stage using climatology. The filled data consisted of the 20-year averages of the data for that period from 2002 to 2021 under each QC method. However, it is important to note that the filled data may not fully represent the true data for that period, which could potentially affect the trend analysis.

However, besides its significance as a physiological parameter that reflects vegetation growth processes, the FPAR is also a crucial factor in terrestrial ecosystem modeling. Therefore, it is essential to thoroughly evaluate the effects of different QC approaches for the FPAR on the simulation results of terrestrial ecosystem models in future research. Despite these uncertainties, our work presents a valuable case for quantifying the impact of remote sensing data products on monitoring VD with different QC methods.

5. Conclusions

In this study, we investigated the impact of QC on vegetation monitoring in the Northern Hemisphere using MODIS C6.1 FPAR time series. Our analyses used linear trend analysis, the MK test, and Sen's slope. The results revealed several important findings. First, the Mixed-QC FPAR was smaller overall than the Main-QC FPAR. In addition, we found that although differences in QC methods led to differences in FPAR values, the trend direction of the long-term series was consistent. Specifically, the interannual GSA FPAR of Northern Hemisphere vegetation showed a consistent and significant ($p < 0.05$) increasing trend. Pixel-by-pixel trend analysis showed that 25.42% of the Mixed-QC FPAR showed a significant increasing trend and 4.3% showed a decreasing trend, whereas the positive and negative trends for the Main-QC FPAR were 27.79% and 4.7%, respectively. This indicates that both QC methods were equally effective in capturing significant trends in vegetation. Finally, although the FPAR time series trend direction was the same for both QC methods, there were differences in the trend magnitude. Specifically, the trend magnitude was higher for Mixed-QC than for Main-QC, and this difference was more pronounced in forests. Overall, the time-series FPAR trends for the two QC methods were in the same direction, but there were differences in values and trend magnitudes. These differences can be attributed to the inclusion of the backup algorithm FPAR with lower inversion accuracy in the Mixed-QC FPAR. However, due to the systematic nature of this difference, its impact on the trend direction is minimal. In conclusion, the results of this study highlight the influence of different QC methods on vegetation trends in the Northern Hemisphere, and although this influence does not reverse the conclusions of the study, it is still recommended to select high-quality inversion results based on quality control documentation or to use internally consistent, high-quality reanalyzed datasets in order to improve the reliability of the study results.

Author Contributions: Conceptualization, K.Y. and J.L.; methodology, X.Z.; software, R.P.; validation, X.Z. and S.G.; formal analysis, X.Z.; investigation, X.Z.; resources, K.Y.; data curation, K.Y.; writing—original draft preparation, K.Y. and X.Z.; writing—review and editing, J.L.; visualization, X.Z.; supervision, K.Y.; project administration, K.Y.; funding acquisition, K.Y. All authors have read and agreed to the published version of the manuscript.

Data Availability Statement: The raw data supporting the conclusions of this article will be made available by the authors upon request.

Conflicts of Interest: The authors declare no conflicts of interest. The funders had no role in the design of the study; in the collection, analysis, or interpretation of the data; in the writing of the manuscript; or in the decision to publish the results.

References

1. Li, H.; Xie, M.; Wang, H.; Li, S.; Xu, M. Spatial heterogeneity of vegetation response to mining activities in resource regions of northwestern China. *Remote Sens.* **2020**, *12*, 3247. [CrossRef]

2. Liu, H.; Yin, Y. Response of forest distribution to past climate change: An insight into future predictions. *Chin. Sci. Bull.* **2013**, *58*, 4426–4436. [CrossRef]

3. Ritchie, J.C. Climate change and vegetation response. *Vegetatio* **1986**, *67*, 65–74. [CrossRef]

4. Liu, Y.; Li, Y.; Li, S.; Motesharrei, S. Spatial and temporal patterns of global NDVI trends: Correlations with climate and human factors. *Remote Sens.* **2015**, *7*, 13233–13250. [CrossRef]

5. Thom, D.; Rammer, W.; Seidl, R. The impact of future forest dynamics on climate: Interactive effects of changing vegetation and disturbance regimes. *Ecol. Monogr.* **2017**, *87*, 665–684. [CrossRef]

6. Ahlström, A.; Xia, J.; Arneth, A.; Luo, Y.; Smith, B. Importance of vegetation dynamics for future terrestrial carbon cycling. *Environ. Res. Lett.* **2015**, *10*, 054019. [CrossRef]

7. Mutuo, P.K.; Cadisch, G.; Albrecht, A.; Palm, C.A.; Verchot, L. Potential of agroforestry for carbon sequestration and mitigation of greenhouse gas emissions from soils in the tropics. *Nutr. Cycling Agroecosyst.* **2005**, *71*, 43–54. [CrossRef]

8. Jiang, D.; Zhang, Y.; Lang, X. Vegetation feedback under future global warming. *Theor. Appl. Climatol.* **2011**, *106*, 211–227. [CrossRef]

9. Liu, Y.; Xue, Y.; MacDonald, G.; Cox, P.; Zhang, Z. Global vegetation variability and its response to elevated CO_2, global warming, and climate variability–a study using the offline SSiB4/TRIFFID model and satellite data. *Earth Syst. Dyn.* **2019**, *10*, 9–29. [CrossRef]

10. Liu, R.; Xiao, L.; Liu, Z.; Dai, J. Quantifying the relative impacts of climate and human activities on vegetation changes at the regional scale. *Ecol. Indic.* **2018**, *93*, 91–99. [CrossRef]

11. Zhang, X.; Huang, X. Human disturbance caused stronger influences on global vegetation change than climate change. *PeerJ* **2019**, *7*, e7763. [CrossRef]

12. Zhang, Y.; Lu, Y.; Song, X. Identifying the Main Factors Influencing Significant Global Vegetation Changes. *Forests* **2023**, *14*, 1607. [CrossRef]

13. Mishra, N.B.; Mainali, K.P. Greening and browning of the Himalaya: Spatial patterns and the role of climatic change and human drivers. *Sci. Total Environ.* **2017**, *587*, 326–339. [CrossRef] [PubMed]

14. Horion, S.; Cornet, Y.; Erpicum, M.; Tychon, B. Studying interactions between climate variability and vegetation dynamic using a phenology based approach. *Int. J. Appl. Earth Obs. Geoinf.* **2013**, *20*, 20–32. [CrossRef]

15. Feng, X.; Fu, B.; Zhang, Y.; Pan, N.; Zeng, Z.; Tian, H.; Lyu, Y.; Chen, Y.; Ciais, P.; Wang, Y. Recent leveling off of vegetation greenness and primary production reveals the increasing soil water limitations on the greening Earth. *Sci. Bull.* **2021**, *66*, 1462–1471. [CrossRef] [PubMed]

16. Jie, T.; Junnan, X.; Yichi, Z.; Weiming, C.; Yuchuan, H.; Chongchong, Y.; Wen, H. Quantitative assessment of the effects of climate change and human activities on grassland NPP in Altay Prefecture. *J. Resour. Ecol.* **2021**, *12*, 743–756. [CrossRef]

17. Sitch, S.; Huntingford, C.; Gedney, N.; Levy, P.; Lomas, M.; Piao, S.; Betts, R.; Ciais, P.; Cox, P.; Friedlingstein, P. Evaluation of the terrestrial carbon cycle, future plant geography and climate-carbon cycle feedbacks using five Dynamic Global Vegetation Models (DGVMs). *Glob. Chang. Biol.* **2008**, *14*, 2015–2039. [CrossRef]

18. Zhang, Y.; Song, C.; Band, L.E.; Sun, G.; Li, J. Reanalysis of global terrestrial vegetation trends from MODIS products: Browning or greening? *Remote Sens. Environ.* **2017**, *191*, 145–155. [CrossRef]

19. Yin, Y.; Ciais, P.; Chevallier, F.; Li, W.; Bastos, A.; Piao, S.; Wang, T.; Liu, H. Changes in the response of the Northern Hemisphere carbon uptake to temperature over the last three decades. *Geophys. Res. Lett.* **2018**, *45*, 4371–4380. [CrossRef]

20. Clark, P.U.; Alley, R.B.; Pollard, D. Northern Hemisphere ice-sheet influences on global climate change. *Science* **1999**, *286*, 1104–1111. [CrossRef]

21. Jin, J.; Wang, Y.; Zhang, Z.; Magliulo, V.; Jiang, H.; Cheng, M. Phenology plays an important role in the regulation of terrestrial ecosystem water-use efficiency in the northern hemisphere. *Remote Sens.* **2017**, *9*, 664. [CrossRef]

22. Wang, S.; Yang, B.; Yang, Q.; Lu, L.; Wang, X.; Peng, Y. Temporal trends and spatial variability of vegetation phenology over the Northern Hemisphere during 1982–2012. *PLoS ONE* **2016**, *11*, e0157134. [CrossRef]

23. Kong, D.; Zhang, Q.; Singh, V.P.; Shi, P. Seasonal vegetation response to climate change in the Northern Hemisphere (1982–2013). *Global. Planet. Chang.* **2017**, *148*, 1–8. [CrossRef]

24. Jeong, S.J.; Ho, C.H.; Gim, H.J.; Brown, M.E. Phenology shifts at start vs. end of growing season in temperate vegetation over the Northern Hemisphere for the period 1982–2008. *Global. Chang. Biol.* **2011**, *17*, 2385–2399. [CrossRef]

25. Zhang, Y.; Piao, S.; Sun, Y.; Rogers, B.M.; Li, X.; Lian, X.; Liu, Z.; Chen, A.; Peñuelas, J. Future reversal of warming-enhanced vegetation productivity in the Northern Hemisphere. *Nat. Clim. Chang.* **2022**, *12*, 581–586. [CrossRef]

26. Fensholt, R.; Langanke, T.; Rasmussen, K.; Reenberg, A.; Prince, S.D.; Tucker, C.; Scholes, R.J.; Le, Q.B.; Bondeau, A.; Eastman, R. Greenness in semi-arid areas across the globe 1981–2007—An Earth Observing Satellite based analysis of trends and drivers. *Remote Sens. Environ.* **2012**, *121*, 144–158. [CrossRef]

27. Frappart, F.; Wigneron, J.-P.; Li, X.; Liu, X.; Al-Yaari, A.; Fan, L.; Wang, M.; Moisy, C.; Le Masson, E.; Aoulad Lafkih, Z. Global monitoring of the vegetation dynamics from the Vegetation Optical Depth (VOD): A review. *Remote Sens.* **2020**, *12*, 2915. [CrossRef]

28. Hussain, S.; Qin, S.; Nasim, W.; Bukhari, M.A.; Mubeen, M.; Fahad, S.; Raza, A.; Abdo, H.G.; Tariq, A.; Mousa, B. Monitoring the dynamic changes in vegetation cover using spatio-temporal remote sensing data from 1984 to 2020. *Atmosphere* **2022**, *13*, 1609. [CrossRef]

29. Yan, K.; Zou, D.; Yan, G.; Fang, H.; Weiss, M.; Rautiainen, M.; Knyazikhin, Y.; Myneni, R.B. A bibliometric visualization review of the MODIS LAI/FPAR products from 1995 to 2020. *J. Remote Sens.* **2021**, *2021*, 7410921. [CrossRef]

30. Zhu, Z.; Piao, S.; Myneni, R.B.; Huang, M.; Zeng, Z.; Canadell, J.G.; Ciais, P.; Sitch, S.; Friedlingstein, P.; Arneth, A. Greening of the Earth and its drivers. *Nat. Clim. Chang.* **2016**, *6*, 791–795. [CrossRef]

31. Sun, Z.; Wang, X.; Yamamoto, H.; Tani, H.; Zhong, G.; Yin, S.; Guo, E. Spatial pattern of GPP variations in terrestrial ecosystems and its drivers: Climatic factors, CO_2 concentration and land-cover change, 1982–2015. *Ecol. Inf.* **2018**, *46*, 156–165. [CrossRef]

32. Piao, S.; Wang, X.; Park, T.; Chen, C.; Lian, X.; He, Y.; Bjerke, J.W.; Chen, A.; Ciais, P.; Tømmervik, H. Characteristics, drivers and feedbacks of global greening. *Nat. Rev. Earth Environ.* **2020**, *1*, 14–27. [CrossRef]

33. Weiss, M.; Baret, F.; Garrigues, S.; Lacaze, R. LAI and fAPAR CYCLOPES global products derived from VEGETATION. Part 2: Validation and comparison with MODIS collection 4 products. *Remote Sens. Environ.* **2007**, *110*, 317–331. [CrossRef]

34. Myneni, R.; Williams, D. On the relationship between FAPAR and NDVI. *Remote Sens. Environ.* **1994**, *49*, 200–211. [CrossRef]

35. Liu, Z.; Notaro, M.; Kutzbach, J.; Liu, N. Assessing global vegetation–climate feedbacks from observations. *J. Clim.* **2006**, *19*, 787–814. [CrossRef]

36. GCOS. The global observing system for climate: Implementation needs. *World Meteorol. Organ.* **2016**, *200*, 316.

37. Sellers, P.J.; Dickinson, R.; Randall, D.; Betts, A.K.; Hall, F.G.; Berry, J.A.; Collatz, G.; Denning, A.; Mooney, H.A.; Nobre, C.A. Modeling the exchanges of energy, water, and carbon between continents and the atmosphere. *Science* **1997**, *275*, 502–509. [CrossRef]

38. Gitelson, A.A.; Gritz, Y.; Merzlyak, M.N. Relationships between leaf chlorophyll content and spectral reflectance and algorithms for non-destructive chlorophyll assessment in higher plant leaves. *J. Plant Physiol.* **2003**, *160*, 271–282. [CrossRef]

39. Liu, R.; Ren, H.; Liu, S.; Liu, Q.; Li, X. Modelling of fraction of absorbed photosynthetically active radiation in vegetation canopy and its validation. *Biosyst. Eng.* **2015**, *133*, 81–94. [CrossRef]

40. Oliphant, A.; Susan, C.; Grimmond, B.; Schmid, H.-P.; Wayson, C.A. Local-scale heterogeneity of photosynthetically active radiation (PAR), absorbed PAR and net radiation as a function of topography, sky conditions and leaf area index. *Remote Sens. Environ.* **2006**, *103*, 324–337. [CrossRef]

41. Tan, C.; Wang, D.; Zhou, J.; Du, Y.; Luo, M.; Zhang, Y.; Guo, W. Remotely assessing fraction of photosynthetically active radiation (FPAR) for wheat canopies based on hyperspectral vegetation indexes. *Front. Plant Sci.* **2018**, *9*, 776. [CrossRef] [PubMed]

42. Zhu, Z.; Bi, J.; Pan, Y.; Ganguly, S.; Anav, A.; Xu, L.; Samanta, A.; Piao, S.; Nemani, R.R.; Myneni, R.B. Global data sets of vegetation leaf area index (LAI) 3g and fraction of photosynthetically active radiation (FPAR) 3g derived from global inventory modeling and mapping studies (GIMMS) normalized difference vegetation index (NDVI3g) for the period 1981 to 2011. *Remote Sens.* **2013**, *5*, 927–948. [CrossRef]

43. Liu, R.; Ren, H.; Liu, S.; Liu, Q.; Yan, B.; Gan, F. Generalized FPAR estimation methods from various satellite sensors and validation. *Agric. For. Meteorol.* **2018**, *260*, 55–72. [CrossRef]

44. Yan, K.; Park, T.; Yan, G.; Chen, C.; Yang, B.; Liu, Z.; Nemani, R.R.; Knyazikhin, Y.; Myneni, R.B. Evaluation of MODIS LAI/FPAR product collection 6. Part 1: Consistency and improvements. *Remote Sens.* **2016**, *8*, 359. [CrossRef]

45. Wang, Y.; Tian, Y.; Zhang, Y.; El-Saleous, N.; Knyazikhin, Y.; Vermote, E.; Myneni, R.B. Investigation of product accuracy as a function of input and model uncertainties: Case study with SeaWiFS and MODIS LAI/FPAR algorithm. *Remote Sens. Environ.* **2001**, *78*, 299–313. [CrossRef]

46. Van Leeuwen, W.J.; Orr, B.J.; Marsh, S.E.; Herrmann, S.M. Multi-sensor NDVI data continuity: Uncertainties and implications for vegetation monitoring applications. *Remote Sens. Environ.* **2006**, *100*, 67–81. [CrossRef]

47. Baret, F.; Weiss, M.; Lacaze, R.; Camacho, F.; Makhmara, H.; Pacholcyzk, P.; Smets, B. GEOV1: LAI and FAPAR essential climate variables and FCOVER global time series capitalizing over existing products. Part1: Principles of development and production. *Remote Sens. Environ.* **2013**, *137*, 299–309. [CrossRef]

48. Myneni, R.B.; Hoffman, S.; Knyazikhin, Y.; Privette, J.; Glassy, J.; Tian, Y.; Wang, Y.; Song, X.; Zhang, Y.; Smith, G. Global products of vegetation leaf area and fraction absorbed PAR from year one of MODIS data. *Remote Sens. Environ.* **2002**, *83*, 214–231. [CrossRef]

49. Yan, K.; Park, T.; Chen, C.; Xu, B.; Song, W.; Yang, B.; Zeng, Y.; Liu, Z.; Yan, G.; Knyazikhin, Y. Generating global products of LAI and FPAR from SNPP-VIIRS data: Theoretical background and implementation. *IEEE Trans. Geosci. Remote Sens.* **2018**, *56*, 2119–2137. [CrossRef]

50. Fuster, B.; Sánchez-Zapero, J.; Camacho, F.; García-Santos, V.; Verger, A.; Lacaze, R.; Weiss, M.; Baret, F.; Smets, B. Quality assessment of PROBA-V LAI, fAPAR and fCOVER collection 300 m products of copernicus global land service. *Remote Sens.* **2020**, *12*, 1017. [CrossRef]

51. Pu, J.; Yan, K.; Zhou, G.; Lei, Y.; Zhu, Y.; Guo, D.; Li, H.; Xu, L.; Knyazikhin, Y.; Myneni, R.B. Evaluation of the MODIS LAI/FPAR algorithm based on 3D-RTM simulations: A case study of grassland. *Remote Sens.* **2020**, *12*, 3391. [CrossRef]

52. Xu, B.; Park, T.; Yan, K.; Chen, C.; Zeng, Y.; Song, W.; Yin, G.; Li, J.; Liu, Q.; Knyazikhin, Y. Analysis of global LAI/FPAR products from VIIRS and MODIS sensors for spatio-temporal consistency and uncertainty from 2012–2016. *Forests* **2018**, *9*, 73. [CrossRef]

53. Yan, K.; Park, T.; Yan, G.; Liu, Z.; Yang, B.; Chen, C.; Nemani, R.R.; Knyazikhin, Y.; Myneni, R.B. Evaluation of MODIS LAI/FPAR product collection 6. Part 2: Validation and intercomparison. *Remote Sens.* **2016**, *8*, 460. [CrossRef]

54. Wang, D.; Liang, S. Improving LAI mapping by integrating MODIS and CYCLOPES LAI products using optimal interpolation. *IEEE J. Sel. Top. Appl. Earth Obs. Remote Sens.* **2013**, *7*, 445–457. [CrossRef]

55. Yang, W.; Shabanov, N.V.; Huang, D.; Wang, W.; Dickinson, R.E.; Nemani, R.R.; Knyazikhin, Y.; Myneni, R.B. Analysis of leaf area index products from combination of MODIS Terra and Aqua data. *Remote Sens. Environ.* **2006**, *104*, 297–312. [CrossRef]

56. Tsalyuk, M.; Kelly, M.; Getz, W.M. Improving the prediction of African savanna vegetation variables using time series of MODIS products. *ISPRS J. Photogramm. Remote Sens.* **2017**, *131*, 77–91. [CrossRef] [PubMed]

57. Hu, S.; Mo, X.; Lin, Z. Optimizing the photosynthetic parameter Vcmax by assimilating MODIS-fPAR and MODIS-NDVI with a process-based ecosystem model. *Agric. For. Meteorol.* **2014**, *198*, 320–334. [CrossRef]

58. He, M.; Kimball, J.S.; Running, S.; Ballantyne, A.; Guan, K.; Huemmrich, F. Satellite detection of soil moisture related water stress impacts on ecosystem productivity using the MODIS-based photochemical reflectance index. *Remote Sens. Environ.* **2016**, *186*, 173–183. [CrossRef]

59. Yang, K.; Yan, K.; Zhang, X.; Zhong, R.; Chi, H.; Liu, J.; Ma, X.; Wang, Y. Assessing FY-3D MERSI-II Observations for Vegetation Dynamics Monitoring: A Performance Test of Land Surface Reflectance. *IEEE Trans. Geosci. Remote Sens.* **2024**, *62*, 1–20. [CrossRef]

60. Wang, J.; Yan, K.; Gao, S.; Pu, J.; Liu, J.; Park, T.; Bi, J.; Maeda, E.E.; Heiskanen, J.; Knyazikhin, Y. Improving the Quality of MODIS LAI Products by Exploiting Spatiotemporal Correlation Information. *IEEE Trans. Geosci. Remote Sens.* **2023**, *61*, 1–19. [CrossRef]

61. Pu, J.; Yan, K.; Roy, S.; Zhu, Z.; Rautiainen, M.; Knyazikhin, Y.; Myneni, R.B. Sensor-independent LAI/FPAR CDR: Reconstructing a global sensor-independent climate data record of MODIS and VIIRS LAI/FPAR from 2000 to 2022. *Earth Syst. Sci. Data Discuss.* **2023**, *2023*, 1–29. [CrossRef]

62. Saleska, S.R.; Didan, K.; Huete, A.R.; da Rocha, H.R. Amazon forests green-up during 2005 drought. *Science* **2007**, *318*, 612. [CrossRef]

63. Samanta, A.; Ganguly, S.; Hashimoto, H.; Devadiga, S.; Vermote, E.; Knyazikhin, Y.; Nemani, R.R.; Myneni, R.B. Amazon forests did not green-up during the 2005 drought. *Geophys. Res. Lett.* **2010**, *37*, L05401. [CrossRef]

64. Samanta, A.; Ganguly, S.; Myneni, R.B. MODIS Enhanced Vegetation Index data do not show greening of Amazon forests during the 2005 drought. *New Phytol.* **2011**, *189*, 11–15. Available online: http://www.jstor.org/stable/40960872 (accessed on 23 January 2024). [CrossRef]

65. Zeng, Y.; Hao, D.; Huete, A.; Dechant, B.; Berry, J.; Chen, J.M.; Joiner, J.; Frankenberg, C.; Bond-Lamberty, B.; Ryu, Y. Optical vegetation indices for monitoring terrestrial ecosystems globally. *Nat. Rev. Earth Environ.* **2022**, *3*, 477–493. [CrossRef]

66. Gawuc, L.; Struzewska, J. Impact of MODIS quality control on temporally aggregated urban surface temperature and long-term surface urban heat island intensity. *Remote Sens.* **2016**, *8*, 374. [CrossRef]

67. Lai, J.; Zhan, W.; Huang, F.; Quan, J.; Hu, L.; Gao, L.; Ju, W. Does quality control matter? Surface urban heat island intensity variations estimated by satellite-derived land surface temperature products. *ISPRS J. Photogramm. Remote Sens.* **2018**, *139*, 212–227. [CrossRef]

68. Sulla-Menashe, D.; Friedl, M.A. *MODIS Collection 6.1 (C61) Land Cover Type Product User Guide*; Usgs: Reston, VA, USA, 2022; Volume 1, p. 20.

69. Peng, S.; Piao, S.; Ciais, P.; Myneni, R.B.; Chen, A.; Chevallier, F.; Dolman, A.J.; Janssens, I.A.; Penuelas, J.; Zhang, G. Asymmetric effects of daytime and night-time warming on Northern Hemisphere vegetation. *Nature* **2013**, *501*, 88–92. [CrossRef] [PubMed]

70. Piao, S.; Friedlingstein, P.; Ciais, P.; Zhou, L.; Chen, A. Effect of climate and CO_2 changes on the greening of the Northern Hemisphere over the past two decades. *Geophys. Res. Lett.* **2006**, *33*. [CrossRef]

71. Myneni, R.; Park, Y. MODIS Collection 6.1 (C6.1) LAI/FPAR Product User's Guide. Available online: https://lpdaac.usgs.gov/documents/926/MOD15_User_Guide_V61.pdf (accessed on 28 January 2024).

72. Hasanpour Kashani, M.; Dinpashoh, Y. Evaluation of efficiency of different estimation methods for missing climatological data. *Stoch. Environ. Res. Risk Assess.* **2011**, *26*, 59–71. [CrossRef]

73. WMO. *World Meteorological Organization Guide to Climatological Practices*; WMO: Geneva, Switzerland, 2018.

74. Kendall, M.G. *Rank Correlation Methods*; Oxford University Press: New York, NY, USA, 1975.

75. Mann, H.B. Nonparametric tests against trend. *Econom. J. Econom. Soc.* **1945**, *13*, 245–259. [CrossRef]

76. Sen, P.K. Estimates of the regression coefficient based on Kendall's tau. *J. Am. Stat. Assoc.* **1968**, *63*, 1379–1389. [CrossRef]

77. Yang, W.; Huang, D.; Tan, B.; Stroeve, J.C.; Shabanov, N.V.; Knyazikhin, Y.; Nemani, R.R.; Myneni, R.B. Analysis of leaf area index and fraction of PAR absorbed by vegetation products from the terra MODIS sensor: 2000–2005. *IEEE Trans. Geosci. Remote Sens.* **2006**, *44*, 1829–1842. [CrossRef]

78. Chen, C.; Park, T.; Wang, X.; Piao, S.; Xu, B.; Chaturvedi, R.K.; Fuchs, R.; Brovkin, V.; Ciais, P.; Fensholt, R. China and India lead in greening of the world through land-use management. *Nat. Sustain.* **2019**, *2*, 122–129. [CrossRef] [PubMed]

79. Knyazikhin, Y. MODIS Leaf Area Index (LAI) and Fraction of Photosynthetically Active Radiation Absorbed by Vegetation (FPAR) Product (MOD15) Algorithm Theoretical Basis Document. Available online: https://lpdaac.usgs.gov/documents/90/MOD15_ATBD.pdf (accessed on 27 January 2024).

80. Clevers, J.; Van Leeuwen, H.J.C.; Verhoef, W. Estimating the fraction APAR by means of vegetation indices: A sensitivity analysis with a combined prospect-sail model. *Remote Sens. Rev.* **1994**, *9*, 203–220. [CrossRef]

81. Rahman, M.M.; Lamb, D.W.; Stanley, J.N. The impact of solar illumination angle when using active optical sensing of NDVI to infer fAPAR in a pasture canopy. *Agric. For. Meteorol.* **2015**, *202*, 39–43. [CrossRef]

82. Liang, S.; Ma, W.; Sui, X.; Wang, M.; Li, H. An Assessment of Relations between Vegetation Green FPAR and Vegetation Indices through a Radiative Transfer Model. *Plants* **2023**, *12*, 1927. [CrossRef] [PubMed]

83. Gao, S.; Zhong, R.; Yan, K.; Ma, X.; Chen, X.; Pu, J.; Gao, S.; Qi, J.; Yin, G.; Myneni, R.B. Evaluating the saturation effect of vegetation indices in forests using 3D radiative transfer simulations and satellite observations. *Remote Sens. Environ.* **2023**, *295*, 113665. [CrossRef]

84. Forzieri, G.; Alkama, R.; Miralles, D.G.; Cescatti, A. Satellites reveal contrasting responses of regional climate to the widespread greening of Earth. *Science* **2017**, *356*, 1180–1184. [CrossRef]

85. Zeng, Z.; Peng, L.; Piao, S. Response of terrestrial evapotranspiration to Earth's greening. *Curr. Opin. Environ. Sustain.* **2018**, *33*, 9–25. [CrossRef]

86. Wu, J.; Wang, D.; Li, L.Z.X.; Zeng, Z. Hydrological feedback from projected Earth greening in the 21st century. *Sustain. Horiz.* **2022**, *1*, 100007. [CrossRef]

87. Li, Y.; Li, Z.-L.; Wu, H.; Zhou, C.; Liu, X.; Leng, P.; Yang, P.; Wu, W.; Tang, R.; Shang, G.-F. Biophysical impacts of earth greening can substantially mitigate regional land surface temperature warming. *Nat. Commun.* **2023**, *14*, 121. [CrossRef]

88. Zhang, Y.; Song, C.; Band, L.E.; Sun, G. No proportional increase of terrestrial gross carbon sequestration from the greening Earth. *J. Geophys. Res. Biogeosci.* **2019**, *124*, 2540–2553. [CrossRef]

89. Faour, G.; Mhawej, M.; Nasrallah, A. Global trends analysis of the main vegetation types throughout the past four decades. *Appl. Geogr.* **2018**, *97*, 184–195. [CrossRef]

90. Lloret, F.; Escudero, A.; Iriondo, J.M.; Martínez-Vilalta, J.; Valladares, F. Extreme climatic events and vegetation: The role of stabilizing processes. *Global. Chang. Biol.* **2012**, *18*, 797–805. [CrossRef]

91. Turner, D.P. Global vegetation monitoring: Toward a sustainable technobiosphere. *Front. Ecol. Environ.* **2011**, *9*, 111–116. [CrossRef]

92. Peng, X.; Zhang, T.; Frauenfeld, O.W.; Wang, S.; Qiao, L.; Du, R.; Mu, C. Northern Hemisphere greening in association with warming permafrost. *J. Geophys. Res. Biogeosci.* **2020**, *125*, e2019JG005086. [CrossRef]

93. Yan, K.; Wang, J.; Peng, R.; Yang, K.; Chen, X.; Yin, G.; Dong, J.; Weiss, M.; Pu, J.; Myneni, R.B. HiQ-LAI: A High-Quality Reprocessed MODIS LAI Dataset with Better Spatio-temporal Consistency from 2000 to 2022. *Earth Syst. Sci. Data Discuss.* **2023**, *2023*, 1–32. [CrossRef]